J. Phys. B: At. Mol. Opt. Phys. **29** (1996) 1979–1994. Printed in the UK

Single-centred calculations of excitation and electron removal in intermediate energy $p + Li^{2+}$ collisions

K A Hall, J F Reading and A L Ford

Center for Theoretical Physics, Physics Department, Texas A&M University, College Station, TX 77843, USA

Received 7 June 1995, in final form 5 February 1996

Abstract. Single-centred finite Hilbert basis set calculations, using bases with a substantial number of orbitals, have previously been shown to accurately reproduce excitation and electron removal cross sections for the single electron $p + H(1s)$, $p + H(n = 2)$, $p + He^+(1s)$ and $p + He^+(n = 2)$ systems. The present paper extends the method's range of application to the $p + Li^{2+}(1s)$ and $p + Li^{2+}(n = 2)$ systems. These cross sections are relevant to controlled nuclear fusion studies. We consider incident projectile energies ranging from 30 keV amu^{-1} to 600 keV amu^{-1}. Cross sections for $1s \rightarrow 2l'$, $3l'$ and $4l'$, 2s and $2p \rightarrow 3l'$ and $4l'$ excitation and for electron removal from the 1s, 2s, and 2p are presented and compared to other theoretical calculations. An interesting feature is exhibited by the $2s \rightarrow 3p$ and 4p excitation cross sections.

1. Introduction

In this paper we present theoretical cross sections obtained by performing a large single-centred finite Hilbert basis set (FHBS) calculation of a fast proton incident on the $n = 1$ and $n = 2$ states of Li^{2+}. In previous papers (Ford *et al* 1993a, b, Hall *et al* 1994) we have demonstrated that the inclusion of large angular momentum states in a single-centred expansion (SCE) about the target yielded accurate excitation and electron removal cross sections. This inclusion of large l allowed us to extend our calculations to lower collision energies where charge transfer is the dominant mechanism for ionization. These high angular momentum basis states allow an adequate description of the important projectile-centred orbitals out to the largest projectile–target separations where transitions occur.

The inclusion of higher angular momentum is desirable to accurately describe excitation from initial excited states to higher-l final states. As the method is unitary, detailed balance is guaranteed.

In our semiclassical impact parameter method, a fast proton, energy 30–600 keV, approaches the Li^{2+} target along a straight-line path with fixed velocity, v_p. This provides a time-dependent perturbation of the target system. The electron can be excited or ionized to a continuum state or a bound projectile state. Our SCE target basis cannot differentiate between a continuum state or a bound projectile state and therefore can only describe electron loss, the sum of ionization and charge capture, from the target. This is the major shortcoming associated with this technique. An advantage is that the SCE presents a simple computational algorithm so that convergence of excitation cross sections with respect to the basis expansion can be successfully achieved.

In collision energy regions where charge transfer is a dominant ionization mechanism, the traditional method of choice is the two-centred expansion (TCE) (Bates and McCarroll

0953-4075/96/101979+16$19.50 © 1996 IOP Publishing Ltd

1958, Wilets and Gallaher 1966, Shakeshaft 1978, Lin *et al* 1978, Winter 1982, Chen *et al* 1994, Slim and Ermolaev 1994). In a TCE calculation, the time-dependent wavefunction for the system is represented by an expansion about both the projectile and target centres using suitable single particle target and projectile basis states. Although the TCE allows for explicit final projectile states, there are some inherent difficulties associated with this technique. Numerical algorithms in general currently limit the basis size to only s, p and d states on both centres. This is due to the fact that the bases on the two centres are not orthogonal and thus the system Hamiltonian must be diagonalized at every time step. Although one might expect rapid convergence for a large enough symmetric basis centred on each centre, this may not be the case. As the bases are increased one runs into the problems linked with linear dependence between the target-centred states and the projectile-centred states.

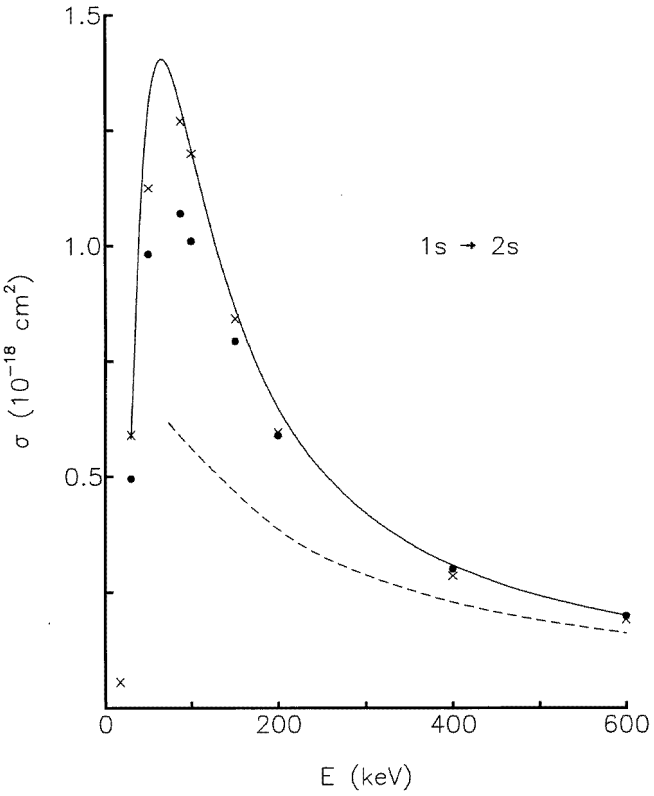

Figure 1. The excitation cross section for 1s $\rightarrow$ 2s as a function of incident projectile energy. The solid curve represents the present single-centred results. The first Born result is represented by the broken curve. The crosses ($\times$) and full circles ($\bullet$) represent alternative basis TCE calculations by Ermolaev and McDowell (1987). Calculations using a 58-state basis ($l \leqslant 3$) centred on the target with the dominant 1s capture state on the projectile are given by the full circles ($\bullet$). The crosses ($\times$) represent calculations using a 19-state basis ($l \leqslant 2$) centred on the target and a 13-state basis ($l \leqslant 2$) on the projectile.

A recent survey (Slim and Ermolaev 1994) of $p + H(1s) \rightarrow p + H^*(n = 2)$ excitation compared the results obtained by using various basis sets in a TCE calculation. Their

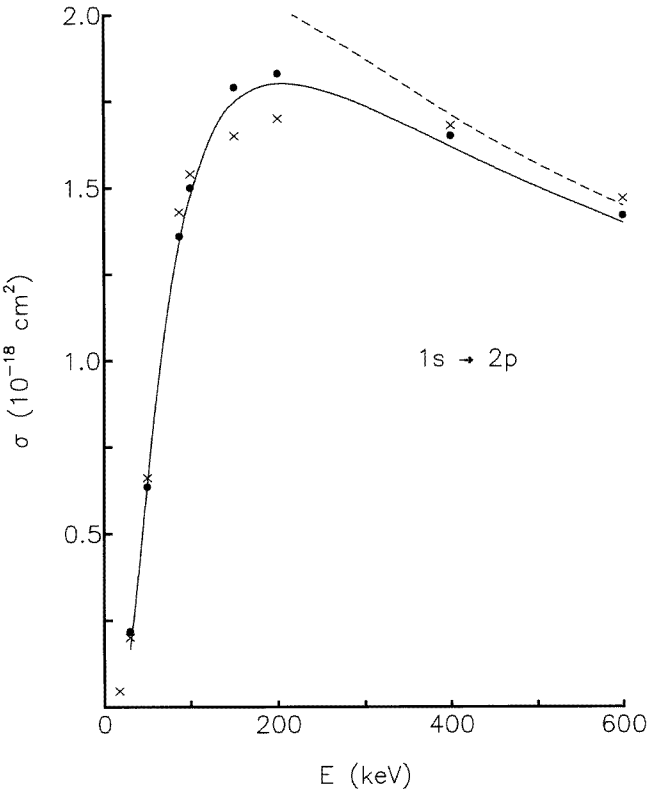

Figure 2. The excitation cross section for 1s → 2p as a function of incident projectile energy. The same notation as in figure 1 is used.

calculations were carried out using four different bases for collision energies of 15–1000 keV. They report accurate results for the intermediate energy range of 30–200 keV using an asymmetric basis consisting of 50 states on the target (up through f states) and the dominant H(1s) capture state on the projectile. Similar calculations using bases with 37 target states and 37 projectile states and 56 target states and 37 projectile states did not exhibit satisfactory convergence in this energy range, although the symmetric 74 state basis did yield accurate results for lower collision energies of 15–30 keV where there is strong coupling between the excitation and charge transfer channels. This problem must be addressed before a single suitable TCE basis can be applied over the entire collision energy range of 15–200 keV (Slim and Ermolaev 1994).

As noted previously, large SCE calculations have been carried out for the $p + H(1s)$, $p+H(n = 2)$, $p+He^+(1s)$ and $p+He^+(n = 2)$ collision systems. The present paper reports similar calculations of the $1s \rightarrow 2l'$, $3l'$ and $4l'$, 2s and $2p \rightarrow 3l'$ and $4l'$ excitation and of the electron removal from 1s, 2s, and 2p for the single electron $p + Li^{2+}$ system. We report individual cross sections for the 2s and 2p initial states along with those averaged over all $n = 2$ initial state sublevels. The per cent deviation, of these cross sections, from the first Born is also given. This allows one to gauge the accuracy of using a simple first Born for a particular transition.

These cross sections are important in fusion plasma research (Phaneuf and Janev 1993). Lithium pellets are used to condition the plasma confinement walls, i.e. to reduce edge influx

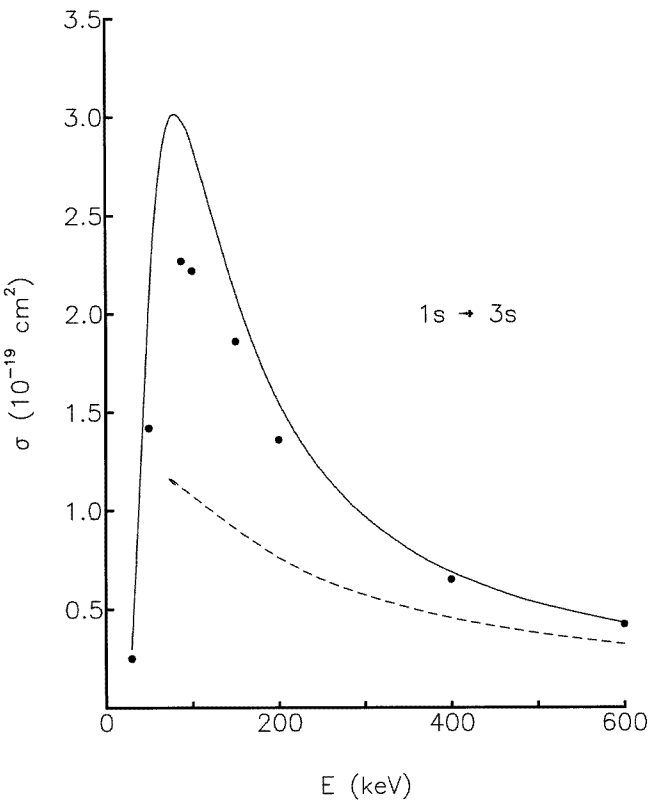

Figure 3. The excitation cross section for 1s → 3s as a function of incident projectile energy. The same notation as in figure 1 is used.

from H and C impurities which reduce confinement times. Lithium pellets are also used in diagnostic procedures, e.g. the measurement of hydrogen ion temperatures in the plasma core after neutral beam injection. Also, electron removal from Li ions and charge transfer to D^+ constitute increased radiative power losses and decreased deuteron fuel densities.

However at this stage we are only beginning the development of a theoretical data base; the cross sections we have presented will find their most useful application in reconciling the results produced by the SCE with those produced by molecular and TCE methods. Once the reliability of these methods is fully understood we may look forward to treating the more directly useful cross sections appropriate to Li atoms and Li^+ ions.

Currently there are no experimental results for any of the above stated transitions. While an experimental preparation of the $Li^{2+}(1s)$ with a merged proton beam may be feasible, it appears unrealistic that an excited Li^{2+} ion target could be prepared. Recently there has been increased theoretical study of the one-electron $p + H$ (Rodríguez and Miraglia 1992, Detleffsen *et al* 1994, Kuang *et al* 1994), $p + He^+$ (Henne *et al* 1993, Errea *et al* 1994a, b, Errea and Sánchez 1994) and $p + Li^{2+}$ (Ast *et al* 1988, Kuang 1991a, b, Bugacov *et al* 1993) collision systems. A very brief outline of the method is given in section 2. In section 3 we present our results and compare these to other theoretical calculations.

Table 1. The λ_i's used in the underlying target basis $\phi_{ilm} = r^l e^{-\lambda_i r} Y_{lm}$ (the λ_i's are dimensionless and have been scaled by $(a_0/Z_T)^{-1}$). Even and odd parity states are formed by linear combinations of the Y_{lm}'s, $d(Y_{lm} \pm Y^*_{lm})$, where

$$d = \begin{cases} \dfrac{1}{\sqrt{2}} & \text{if } m \neq 0; \\ \dfrac{1}{2} & m = 0. \end{cases}$$

The eigenenergies (in au) associated with each state through $l_{\max} = 6$ (i states) are also listed. The target Hamiltonian has been shifted such that $\epsilon = 0$ corresponds to the ground state. The eigenenergies, E_ϵ, conventionally defined so that the ionization threshold is at zero, are given by $E_\epsilon = (\epsilon - 0.5)\ Z_T^2$.

λ_i
$\lambda_1 = 0.1708$
$\lambda_{2,13} = 0.2135 \mp 0.07794$i
$\lambda_{3,12} = 0.3080 \mp 0.21130$i
$\lambda_{4,11} = 0.4324 \mp 0.39430$i
$\lambda_{5,10} = 0.6222 \mp 0.61220$i
$\lambda_{6,9} = 0.9743 \mp 0.82770$i
$\lambda_{7,8} = 1.630 \mp 0.81550$i

	$\epsilon_{\text{s-states}}$	$\epsilon_{\text{p-states}}$	$\epsilon_{\text{d-states}}$	$\epsilon_{\text{f-states}}$	$\epsilon_{\text{g-states}}$	$\epsilon_{\text{h-states}}$	$\epsilon_{\text{i-states}}$
ϵ_1	0.0000	0.3750	0.4444	0.4687	0.4800	0.4861	0.4899
ϵ_2	0.3750	0.4444	0.4687	0.4800	0.4863	0.4907	0.4944
ϵ_3	0.4444	0.4687	0.4800	0.4868	0.4927	0.4980	0.5025
ϵ_4	0.4687	0.4803	0.4890	0.4980	0.5067	0.5144	0.5213
ϵ_5	0.4812	0.4933	0.5067	0.5189	0.5289	0.5364	0.5417
ϵ_6	0.5006	0.5214	0.5407	0.5567	0.5702	0.5825	0.5946
ϵ_7	0.5427	0.5731	0.5963	0.6127	0.6234	0.6307	0.6331
ϵ_8	0.6220	0.6621	0.6884	0.7068	0.7220	0.7369	0.7543
ϵ_9	0.7662	0.8125	0.8342	0.8437	0.8460	0.8425	0.8345
ϵ_{10}	1.043	1.084	1.091	1.088	1.086	1.089	1.100
ϵ_{11}	1.645	1.621	1.555	1.489	1.427	1.371	1.320
ϵ_{12}	3.378	2.958	2.623	2.386	2.219	2.102	2.026
ϵ_{13}	13.04	8.081	5.829	4.588	3.814	3.293	2.926

2. Experimental method

The calculations were carried out using the same methods and basis states used in Ford *et al* (1993a, b) and Hall *et al* (1994). The projectile, which follows a straight-line constant velocity path, $\boldsymbol{R} = (\boldsymbol{B}, v_p t)$, provides a time-dependent perturbation $V(|\boldsymbol{R} - \boldsymbol{r}|, t)$ of the target atom. The state vector $\underline{\psi}_l(t)$, in the interaction picture, is propagated through time using the time-development operator U-matrix approach. An accurate calculation of each transition amplitude requires an ample number of time grid points and sufficiently small time steps to satisfy the first Magnus approximation (Pechukas and Light 1966, Martir 1981). Using an underlying basis of the form $\phi_{ilm} = r^l e^{-\lambda_i r} Y_{lm}$, where $\lambda_i \in C$, the target Hamiltonian can be diagonalized to produce eigenvector basis states. The basis was constructed with 13 radial functions for each angular momentum value, l. For each l pseudostates were produced that represent the low-lying bound states and that provide a discrete representation of the continuum. The λ_i's are chosen such that the $\Re(\lambda_i) > 0$ and $\lambda_1 \in \Re$ with the remaining λ_i's forming conjugate pairs. No optimization of the λ_i parameters is performed. Rather, they are selected by an algorithm (Ford *et al* 1977) that

allows for a systematic increase in the number of λ_i while avoiding linear dependence in the basis. The overall scale of the set of λ_i is chosen to give an energy spectrum for the target hamiltonian when it is diagonalized on the basis that represents well the bound levels and portion of the ionization continuum that are important for the collisions being studied.

The eigenenergies and λ_i's used in our 13-state basis are shown in table 1. For s partial waves ($l = 0$), our 13 state basis resulted in five bound states and eight continuum states extending up to 3.1 keV above the ionization threshold. The largest angular momentum included, i partial waves ($l = 6$), had two bound states and 11 continuum states reaching a maximum of 594 eV above the ionization threshold. A more thorough discussion of the U-matrix approach can be found in Fitchard *et al* (1977) and Ford *et al* (1977).

3. Results

Several convergence tests have been performed to gauge the accuracy of the target-centred basis results. One test is the convergence in $l_{\max}$, the maximum angular momentum l included in the underlying basis. As the collision energy is decreased, and the charge transfer cross section increases, a higher $l_{\max}$ is necessary to adequately describe projectile-centred orbitals for maximum projectile–target separations. A compilation of these results for incident projectile energies $E = 25$, 50 and 100 keV is presented in table 2.

Table 2. The convergence in $l_{\max}$ for excitation and electron removal cross sections. The first column indicates the change in σ due to increasing the underlying basis from $l_{\max} = 4$ (g states) to $l_{\max} = 5$ (h states). The second column shows the variation in σ effected by increasing the basis from $l_{\max} = 5$ (h states) to $l_{\max} = 6$ (i states). Projectile velocities, v_p are scaled by the target K-shell velocity.

$E = 30$ keV ($v_p = 0.365$)	$l_{\max} = 5$	$l_{\max} = 6$
$1s \rightarrow n' = 2$	−3.5%	−1.5%
$1s \rightarrow n' = 3$	−7.7%	−6.1%
$1s \rightarrow n' = 4$	−12%	−10%
$n = 2 \rightarrow n' = 3$	−6.5%	−4.5%
$n = 2 \rightarrow n' = 4$	−8.6%	−8.0%
$Li^{2+}(1s)$ e^- removal	+20%	+16%
$Li^{2+}(n = 2)$ e^- removal	+27%	+19%
$E = 50$ keV ($v_p = 0.472$)	$l_{\max} = 5$	$l_{\max} = 6$
$1s \rightarrow n' = 2$	−1.0%	−0.8%
$1s \rightarrow n' = 3$	−4.5%	−3.4%
$1s \rightarrow n' = 4$	−7.3%	−5.6%
$n = 2 \rightarrow n' = 3$	−4.8%	−2.6%
$n = 2 \rightarrow n' = 4$	−8.4%	−4.7%
$Li^{2+}(1s)$ e^- removal	+11%	+8.0%
$Li^{2+}(n = 2)$ e^- removal	+20%	+10%
$E = 100$ keV ($v_p = 0.667$)	$l_{\max} = 5$	$l_{\max} = 6$
$1s \rightarrow n' = 2$	−0.6%	−0.4%
$1s \rightarrow n' = 3$	−1.8%	−1.2%
$1s \rightarrow n' = 4$	−2.6%	−1.7%
$n = 2 \rightarrow n' = 3$	−1.7%	−0.8%
$n = 2 \rightarrow n' = 4$	−3.1%	−1.1%
$Li^{2+}(1s)$ e^- removal	+4.9%	+2.3%
$Li^{2+}(n = 2)$ e^- removal	+10%	+4.1%

The convergence with respect to angular momentum is given for the $1s \rightarrow n' = 2$, 3 and 4, the $n = 2 \rightarrow n' = 3$ and 4 excitation and the electron removal from the 1s and $n = 2$. The first column indicates the percentage change in the cross section σ when the underlying basis is increased from $l_{max} = 4$ (g states) to $l_{max} = 5$ (h states). The second column reports the change in σ when l_{max} is increased from $l_{max} = 5$ to $l_{max} = 6$. The $1s \rightarrow n'$ and $n = 2 \rightarrow n'$ cross sections are, in general, better converged than the individual 1s and $2l \rightarrow n'l'$ cross sections, with the largest error associated with the smallest cross sections. We were unable to obtain suitable converged results for energies below 30 keV with the current algorithm. The convergence in l_{max} and also in the number of time integration mesh points appears to be the difficulty.

For the $p + He^+$ calculations of Hall *et al* (1994) the lowest energy at which reasonable convergence could be obtained was 25 keV. The projectile velocity to 1s electron velocity ratio at 25 keV for $p + He^+$ is the same as for 56 keV $p + Li^{2+}$, so the single-centred method was found to give converged results at lower scaled energies for this more asymmetric collision. The $Li^{2+}(2s)$ and $Li^{2+}(2p)$ electron removal cross sections, at these lower target K-shell scaled velocities, are less adequately converged. This behaviour suggests that perhaps even larger l target bases must be used to adequately describe electron removal from these initial excited states of Li^{2+}.

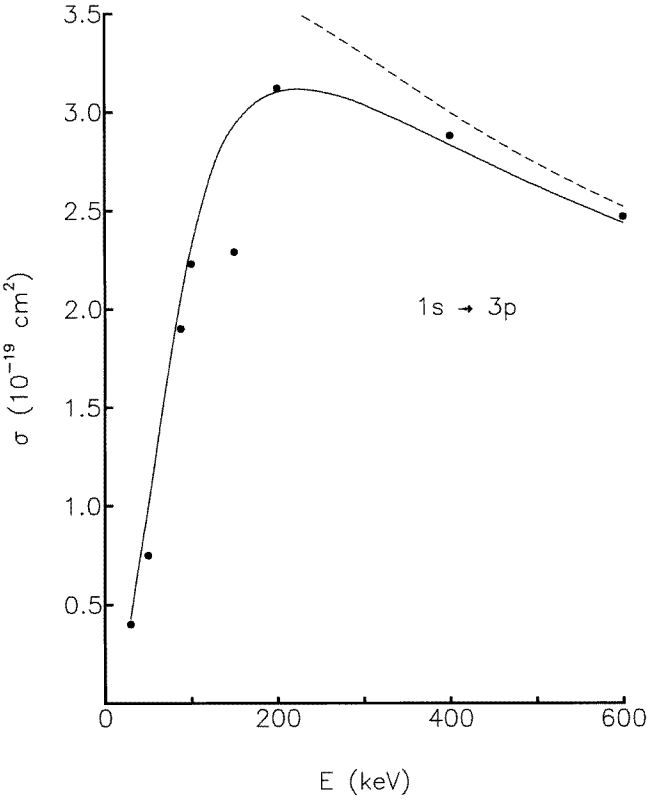

Figure 4. The excitation cross section for $1s \rightarrow 3p$ as a function of incident projectile energy. The same notation as in figure 1 is used.

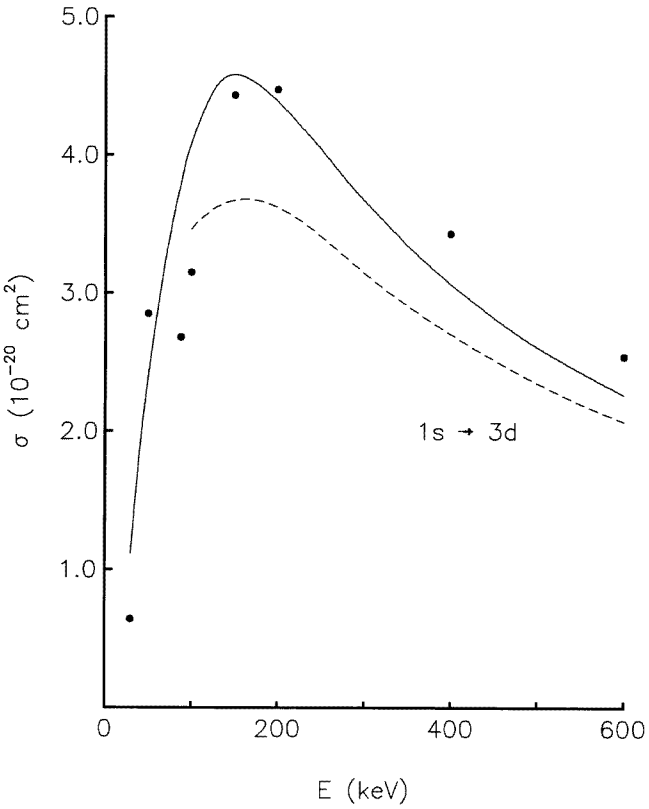

Figure 5. The excitation cross section for 1s → 3d as a function of incident projectile energy. The same notation as in figure 1 is used.

Cross sections for 1s → 2l', 3l' and 4l' are presented in table 3. The 2s and 2p → 3l′ and 4l′ cross sections are presented in table 4. The 2l → $n'l'$ cross sections are summed over final state m' values and averaged over the initial state m values, while the $\sigma(n = 2 \rightarrow n')$ cross sections are averaged over the initial state l value. Individual $\sigma(1s \rightarrow n'l'm')$ and $\sigma(2lm \rightarrow n'l'm')$ cross sections, for laboratory energies of 30–3000 keV, have been tabulated and can be provided upon request.

In addition to listing the individual excitation cross sections, tables 3 and 4 also show the approach of these cross sections to the first Born approximation. The dipole forbidden transitions approach the first Born much more slowly than do the dipole allowed ones for the 1s → 2l' and 3l' excitation cross sections. The 1s → ns and 1s → n'd cross sections approach the first Born from above and the 1s → n'p cross sections approach the first Born from below, so the 1s → $n' = 2$ and 1s → $n' = 3$ summed cross sections approach the first Born more rapidly than do the individual $n'l'$ cross sections. The 1s → 4f cross section is much smaller than the other $n' = 4$ cross sections. The cross sections for the $n = 2$ initial state are closer to the first Born at each energy than are the $n = 1$ cross sections.

Our results for excitation from the initial 1s → 2s, 2p, 3s, 3p and 3d are compared with a TCE calculation (Ermolaev and McDowell 1987) in figures 1–5 respectively. The results from Ermolaev and McDowell (1987) represent close-coupled atomic orbital model calculations using different size bases on the target and the projectile. The first is a 32-state

Table 3. Cross sections for $1s \rightarrow 2l'$ (in units of 10^{-19} cm^2), $1s \rightarrow 3l'$ (10^{-20} cm^2) and $1s \rightarrow 4l'$ (10^{-20} cm^2) as a function of the collision energy. Also the approach of the $1s \rightarrow 2l'$, $3l'$ and $4l'$ excitation cross sections to the first Born as the collision energy E is increased. For $E \geqslant$ 250 keV the cross section σ and the per cent deviation from the first Born, $\Delta = (\sigma - \sigma_{\text{Born}})/\sigma_{\text{Born}}$, are given. The 2p, 3p, 3d, 4p, 4d and 4f cross sections are summed over all the degenerate sublevels of the final state.

	30 keV	40 keV	60 keV	80 keV	100 keV	125 keV	150 keV	200 keV
$1s \rightarrow 2s$	5.83	10.4	13.9	13.5	12.1	10.2	8.65	6.48
$1s \rightarrow 2p$	1.67	3.85	8.79	12.4	14.7	16.6	17.5	18.0
$1s \rightarrow n' = 2$	7.49	14.2	22.7	25.9	26.8	26.8	26.1	24.5
$1s \rightarrow 3s$	2.98	11.8	26.5	30.1	28.5	24.8	21.0	15.5
$1s \rightarrow 3p$	4.29	7.21	12.9	18.7	23.2	27.1	29.3	31.0
$1s \rightarrow 3d$	1.12	1.84	2.85	3.57	4.09	4.46	4.58	4.38
$1s \rightarrow n' = 3$	8.39	20.9	42.3	52.4	55.8	56.4	54.9	50.9
$1s \rightarrow 4s$	0.254	2.14	8.26	10.9	11.0	9.83	8.46	6.28
$1s \rightarrow 4p$	1.41	3.06	4.76	6.29	7.76	9.23	10.1	10.9
$1s \rightarrow 4d$	0.590	1.09	1.55	1.79	1.98	2.13	2.20	2.10
$1s \rightarrow 4f$	0.096	0.15	0.18	0.19	0.18	0.16	0.15	0.11
$1s \rightarrow n' = 4$	2.35	6.44	14.8	19.2	20.9	21.4	20.9	19.4

	250 keV		300 keV		400 keV		500 keV		600 keV	
	σ	Δ	σ	Δ	σ	Δ	σ	Δ	σ	Δ
$1s \rightarrow 2s$	5.11	+55%	4.21	+46%	3.08	+35%	2.42	+28%	1.98	+23%
$1s \rightarrow 2p$	17.8	−8.8%	17.4	−7.3%	16.2	−5.4%	15.0	−4.2%	14.0	−3.4%
$1s \rightarrow n' = 2$	22.9	+0.5%	21.6	−0.2%	19.3	−0.6%	17.4	−0.7%	16.0	−0.7%
$1s \rightarrow 3s$	12.0	+84%	9.68	+70%	6.87	+52%	5.28	+41%	4.27	+33%
$1s \rightarrow 3p$	31.0	−9.7%	30.4	−7.8%	28.3	−5.5%	26.3	−4.2%	24.4	−3.3%
$1s \rightarrow 3d$	4.04	+19%	3.67	+17%	3.06	+13%	2.61	+11%	2.26	+9.4%
$1s \rightarrow n' = 3$	47.0	+6.2%	43.8	+4.7%	38.2	+2.8%	34.2	+1.9%	30.9	+1.4%
$1s \rightarrow 4s$	4.83	+99%	3.87	+83%	2.71	+61%	2.06	+48%	1.66	+39%
$1s \rightarrow 4p$	11.0	−11%	10.8	−8.6%	10.1	−5.9%	9.37	−4.4%	8.70	−3.5%
$1s \rightarrow 4d$	1.92	+19%	1.74	+17%	1.45	+13%	1.23	+11%	1.07	+8.9%
$1s \rightarrow 4f$	0.079	+129%	0.063	+103%	0.044	+73%	0.033	+54%	0.026	+41%
$1s \rightarrow n' = 4$	17.8	+8.8%	16.5	+6.6%	14.3	+4.2%	12.7	+3.0%	11.5	+2.2%

Table 4. Cross sections for 2s, 2p $\rightarrow 3l'$ and $4l'$ excitation (in units of 10^{-18} cm^2) as a function of the collision energy. Also the approach of the 2s, 2p $\rightarrow 3l'$ and $4l'$ excitation cross sections to the first Born as the collision energy E is increased. Δ is the percent deviation from the first Born, as in Table 3. In each case the cross sections are summed over all the degenerate sublevels of the indicated final state and averaged over the degenerate sublevels of the initial state.

	30 keV	40 keV	60 keV	80 keV	100 keV	125 keV	150 keV	200 keV
2s $\rightarrow$ 3s	18.4	18.7	16.1	13.5	11.6	9.75	8.38	6.48
2s $\rightarrow$ 3p	16.7	13.9	14.3	15.9	17.0	17.6	17.8	17.5
2s $\rightarrow$ 3d	54.4	51.0	43.8	37.5	32.4	27.5	24.0	19.0
2s $\rightarrow n' = 3$	89.5	83.7	74.1	66.9	61.0	54.9	50.2	42.9
2p $\rightarrow$ 3s	8.08	4.77	2.36	1.58	1.23	1.00	0.874	0.724
2p $\rightarrow$ 3p	35.2	28.7	21.0	16.7	13.8	11.3	9.51	7.22
2p $\rightarrow$ 3d	44.3	49.8	55.1	56.0	54.9	52.5	50.0	45.0
2p $\rightarrow n' = 3$	87.6	83.3	78.5	74.2	69.9	64.8	60.4	53.0
$n = 2 \rightarrow n' = 3$	88.1	83.4	77.4	72.4	67.7	62.3	57.8	50.5
2s $\rightarrow$ 4s	3.42	4.19	3.80	3.17	2.67	2.21	1.87	1.41
2s $\rightarrow$ 4p	5.52	3.55	2.60	2.69	2.89	3.05	3.13	3.12
2s $\rightarrow$ 4d	8.73	7.55	5.94	4.94	4.22	3.56	3.10	2.41
2s $\rightarrow$ 4f	5.48	5.86	5.00	3.99	3.23	2.56	2.11	1.57
2s $\rightarrow n' = 4$	23.1	21.2	17.3	14.8	13.0	11.4	10.2	8.51
2p $\rightarrow$ 4s	3.45	1.91	0.765	0.445	0.317	0.239	0.198	0.154
2p $\rightarrow$ 4p	9.43	7.72	5.27	3.97	3.16	2.51	2.08	1.53
2p $\rightarrow$ 4d	7.33	8.15	8.90	8.97	8.74	8.29	7.84	6.94
2p $\rightarrow$ 4f	3.12	3.51	3.60	3.31	2.96	2.57	2.25	1.78
2p $\rightarrow n' = 4$	23.3	21.3	18.5	16.7	15.2	13.6	12.4	10.4
$n = 2 \rightarrow n' = 4$	23.3	21.3	18.2	16.2	14.6	13.1	11.8	9.94

Table 4. Continued.

	250 keV		300 keV		400 keV		500 keV		600 keV	
	σ	Δ	σ	Δ	σ	Δ	σ	Δ	σ	Δ
2s → 3s	5.26	+9.8%	4.41	+9.0%	3.32	+7.6%	2.66	+6.5%	2.21	+5.6%
2s → 3p	16.6	−11%	15.8	−9.2%	14.1	−6.4%	12.6	−4.9%	11.5	−3.9%
2s → 3d	15.5	+1.3%	13.1	+1.4%	9.96	+1.5%	8.03	+1.4%	6.72	+1.3%
2s → $n' = 3$	37.4	−3.7%	33.3	−3.0%	27.3	−2.1%	23.3	−1.6%	20.4	−1.3%
2p → 3s	0.632	−3.5%	0.570	−4.0%	0.483	−3.9%	0.424	−3.5%	0.379	−3.1%
2p → 3p	5.79	+9.2%	4.83	+7.8%	3.61	+6.1%	2.88	+4.9%	2.40	+4.1%
2p → 3d	40.6	−6.9%	37.1	−5.5%	31.6	−3.8%	27.5	−2.9%	24.5	−2.3%
2p → $n' = 3$	47.1	−5.1%	42.5	−4.1%	35.7	−2.9%	30.8	−2.2%	27.3	−1.8%
$n = 2 \rightarrow n' = 3$	44.6	−4.8%	40.2	−3.9%	33.6	−2.8%	29.0	−2.1%	25.5	−1.7%
2s → 4s	1.13	+20%	0.934	+18%	0.690	+14%	0.545	+12%	0.450	+9.8%
2s → 4p	2.98	−13%	2.84	−10%	2.54	−7.2%	2.28	−5.4%	2.08	−4.3%
2s → 4d	1.96	−0.9%	1.65	−0.4%	1.25	+0.0%	1.00	+0.2%	0.839	+0.3%
2s → 4f	1.22	+15%	0.992	+12%	0.722	+8.6%	0.567	+6.4%	0.467	+5.0%
2s → $n' = 4$	7.29	−1.4%	6.41	−1.3%	5.20	−1.0%	4.40	−0.9%	3.84	−0.7%
2p → 4s	0.130	−2.9%	0.114	−4.0%	0.0947	−4.4%	0.0820	−4.0%	0.0729	−3.6%
2p → 4p	1.21	+15%	0.993	+13%	0.733	+9.2%	0.580	+7.2%	0.480	+5.8%
2p → 4d	6.20	−6.0%	5.62	−4.7%	4.72	−3.3%	4.09	−2.4%	3.62	−1.9%
2p → 4f	1.45	+13%	1.23	+11%	0.930	+8.6%	0.746	+6.9%	0.623	+5.6%
2p → $n' = 4$	8.99	−0.8%	7.95	−0.6%	6.48	−0.4%	5.49	−0.3%	4.79	−0.3%
$n = 2 \rightarrow n' = 4$	8.57	−0.9%	7.57	−0.8%	6.16	−0.6%	5.22	−0.4%	4.55	−0.4%

basis with 19 states on the target and 13 states on the projectile. This basis consists of s, p and d states on both centres with 12 and 4 continuum states on the target and projectile centres respectively. The second is a 59-state basis with 58 states of $l \leqslant 3$ centred on the target and the dominant 1s capture state on the projectile. Results using both bases were reported for 1s $\rightarrow$ 2s and 2p excitation. Excitation cross sections for 1s $\rightarrow$ 3l and 1s $\rightarrow \sum_{n\geqslant 4} nl$ were reported for the larger 59-state basis only.

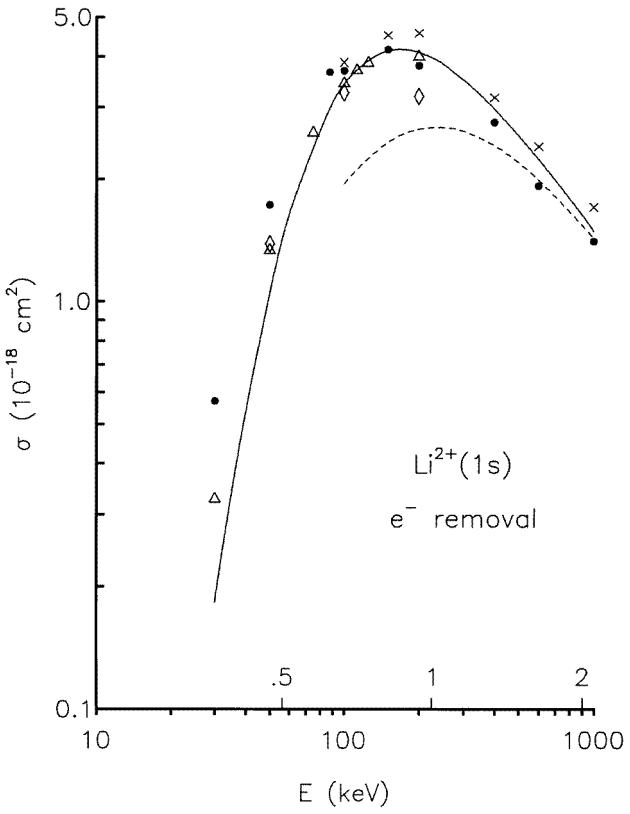

Figure 6. The $Li^{2+}(1s)$ electron removal cross section. The solid curve is the present single-centred result. Cross sections for energies below 60 keV represent 13-state 'extended' basis results, as noted in the text. The first Born result is represented by the broken curve. The crosses (×) and full circles (•) represent sums of the total capture and ionization TCE results of Ermolaev and McDowell (1987). The crosses (×) portray total capture and ionization using the 32-state basis. The full circles (•) represent total capture using the 32-state basis and ionization using the 59-state basis. The triangles (△) are the coupled-states Sturmian results of Winter (1987). Coupled-channel calculations using the 'perturbative one-and-a-half-centre' (POHCE) formulation (Ford *et al* 1982) are represented by the diamonds (◇). Abscissae for projectile velocities, scaled by the target K-shell velocity, are shown for reference.

The smaller 32-state basis (AO32) 1s $\rightarrow$ 2s excitation results are larger than the 59-state basis (AO59) results for energies 200 keV and below. The AO32 results are in good agreement with ours over the 30–600 keV range depicted in figure 1, except at 50 keV where our result is 15% higher. The AO59 results are below ours throughout the energy

Table 5. Cross sections for electron removal from $Li^{2+}(1s)$, $Li^{2+}(2l)$ and $Li^{2+}(n = 2)$ (in units of 10^{-18} cm^2) as a function of the collision energy. For the 2p initial state the cross section is averaged over the three m components of this state. The averaging over the initial $2l$ states gives $\sigma(n = 2) = \frac{1}{4}(\sigma(2s) + 3\sigma(2p))$. Δ is the percent deviation from the first Born, as in table 3. Energies marked with a † represent results using a 13-state 'extended' basis, as noted in the text.

	30 keV†	40 keV†	60 keV†	80 keV	100 keV	125 keV	150 keV	200 keV
$\sigma(1s)$	0.183	0.540	1.64	2.63	3.43	3.91	4.13	4.09
$\sigma(2s)$	70.5	74.2	63.1	52.6	44.6	36.0	31.2	24.4
$\sigma(2p)$	88.2	104	92.3	71.6	58.8	46.5	39.6	30.0
$\sigma(n = 2)$	83.8	96.8	85.0	66.8	55.2	43.9	37.5	28.6

	250 keV		300 keV		400 keV		500 keV		600 keV	
	σ	Δ	σ	Δ	σ	Δ	σ	Δ	σ	Δ
$\sigma(1s)$	3.84	+42%	3.50	+34%	2.97	+23%	2.56	+16%	2.24	+12%
$\sigma(2s)$	20.0	+4.8%	16.3	+2.8%	12.7	+0.6%	10.4	−0.5%	8.90	−1.2%
$\sigma(2p)$	24.2	+7.0%	19.8	+4.3%	15.2	+1.5%	12.4	+0.1%	10.5	−0.6%
$\sigma(n = 2)$	23.2	+6.5%	18.9	+4.0%	14.6	+1.3%	11.9	−0.0%	10.1	−0.8%

range of the peak, $50 - 100$ keV, but agree with our results for energies above 200 keV. Our 1s $\rightarrow$ 2p excitation results, depicted in figure 2, agree well with both the AO32 and AO59 results. Our single-centred cross section values lie between the AO32 and AO59 results at the peaks. A comparison between our results and the AO59 TCE calculation for 1s $\rightarrow$ 3s excitation, shown in figure 3, portrays agreement except at the peak region where our peak is approximately 33% larger. Figure 4 shows excellent agreement between these two calculations except at the 150 keV energy where our cross section is above the AO59 result. Our 1s $\rightarrow$ 3d excitation results, shown in figure 5, are in fair agreement with the AO59 results but agree well near the peak for energies between 150–200 keV. In general our results for 1s $\rightarrow$ n'p agree well with the TCE results of Ermolaev and McDowell (1987) while our 1s $\rightarrow$ ns cross sections exhibit larger peak values than the AO59 calculations. The AO32 calculations gave the best overall agreement with our results for the 1s $\rightarrow$ 2l excitation cross sections.

An interesting feature is exhibited by the 2s $\rightarrow$ 3p and 4p excitation cross sections. Of all the reported cross sections only these two display an apparent local minimum as the projectile energy is decreased (see table 4). As a special convergence test, 'extended' bases, with 13 and 17-states for each l, were created. These bases used λ_i's (see table 1) that were decreased by a factor of two. The original basis states were specifically designed for symmetric systems such as protons incident upon hydrogen. Recalling that all lengths are scaled to the target K-shell radius, it will be observed that although the basis is optimal for states centred on the Li^{2+} target it is incorrectly scaled for the proton projectile states. Extending the *range* of the basis reflects an attempt to come to some compromise between the scales mandated by the different charges of the two heavy nuclei in the collision.

A comparison between results using the original and 'extended' 13-state bases indicated a negligible change in all the excitation cross sections. In particular the local minima, exhibited by the 2s $\rightarrow$ 3p and 4p excitation cross sections, still remain. The origin of this structure is not clear. If, as might be guessed, it is a reflection of the nodal multiplicity present in the initial and final states it should be present in a first Born result. As the Born result is particularly easy to calculate we were able to look for minima on a much finer energy mesh than was possible for the full results. No minima were to be found. Also we investigated using our full coupled channel code cross sections on a finer energy mesh than presented here. No indication of missing minima were found.

Whereas the excitation cross sections did not change with the 'extended' 13-state basis, the electron loss results showed significant increases at the lowest projectile energies. Specifically, at 30 keV, the 13-state 'extended' basis 1s, 2s and 2p electron loss results increased by 31%, 17% and 21% respectively. At 80 keV, the 1s, 2s and 2p electron loss cross sections increased only 4.6%, 0.1% and 4.1% respectively. Since the electron removal cross sections changed significantly at the lowest energy, a comparison between 13-state and 17-state 'extended' basis results was performed. There was no significant change in the 2s electron loss cross section; increases of just 3.8% (1s) and 7.6% (2p) for the electron loss cross sections were noted at 30 keV. At 40 keV these increases were both less than 3%. Negligible changes were identified for the excitation cross sections.

This investigation leads us to conjecture that an 'extended' basis may be preferable at the low energy end of our results. It also indicates that we might be approaching a low energy limit to the SCE method. We leave these questions for further work. Figure 6 shows a comparison between our single-centred results for electron removal from Li^{2+}(1s) and those of Ermolaev and McDowell (1987), Winter (1987) and Ford *et al* (1982). A compilation of our results for electron removal from Li^{2+}(1s), Li^{2+}(2l) and Li^{2+}($n = 2$) is given in table 5. The cross sections for 30, 40 and 60 keV represent 13-state 'extended'

basis calculations. Results for ionization were given for both the 32-state basis (AO32) and the 59-state basis (AO59) calculations performed by Ermolaev and McDowell (1987). Calculations for total electron capture were presented for the AO32 basis and capture to the 1s projectile state using the AO59 basis. Figure 6 depicts two different sums for electron removal where both sums use the AO32 basis total capture results but different bases for the ionization component. The coupled-Sturmian TCE calculations (Winter 1987) shown in figure 6 represent calculations using bases with 45 states for energies 30–75 keV and 36-states for energies 100–200 keV. Both bases have approximately the same number of states on each centre. The perturbative 'one-and-a-half-centred' expansion (POHCE) results of Ford *et al* (1982) are also shown in figure 6 at laboratory energies 50, 100 and 200 keV. For energies 200 keV and above the current single-centred results lie between the TCE results using the AO32 and AO59 ionization results. The AO32 basis ionization results converge to those using the AO59 basis for energies below 100 keV. Thus electron removal results using the AO32 basis for energies below 100 keV are not shown in figure 6. Our single-centred results are in poor agreement with the TCE results of Ermolaev and McDowell (1987) for energies below 100 keV. At the lowest energy of 30 keV our results are a factor of 3.1 smaller. The coupled-Sturmian TCE results of Winter (1987) are in good agreement with our results for energies 75 keV and above. Our results are also significantly smaller at energies below 75 keV. At the lowest energy reported, 30 keV, our single-centred results are a factor of 1.8 smaller than those of Winter (1987). The POHCE results of Ford *et al* are comparable to those of Winter (1987) at 50 keV and 100 keV. The POHCE results are smaller than all the reported theoretical results at 200 keV. At 200 keV the POHCE result is 28% lower than the current SCE result which represents a median value between the other TCE calculations at this energy. The $Li^{2+}(1s)$ electron removal cross section, using our original 13-state basis, increased by 19% when $l_{max} = 5$ was increased to $l_{max} = 6$ (see table 2). Thus the inclusion of even larger angular momentum in the underlying target basis would not appear to rectify the major discrepancy between our SCE results and the two TCE results (Ermolaev and McDowell 1987, Winter 1987) at these lower energies.

There is a need for experimental data to gauge these theoretical calculations for both the $Li^{2+}(1s)$ and $Li^{2+}(n = 2)$ initial state configurations. As noted previously a $Li^{2+}(1s)$ target preparation might be feasible, while the excited state configuration appears unrealistic. To our knowledge this is the first publication of excitation and electron removal for the excited $Li^{2+}(n = 2)$ initial states. Our hope is that the present work will stimulate further study of this basic ion–atom collision system.

Acknowledgments

This work was supported by a grant from the US National Science Foundation PHY-9318449 and by the US Department of Energy under grant DE-FG05-92ER54174.

References

Ast H, Lüdde H J and Dreizler R M 1988 *J. Phys. B: At. Mol. Opt. Phys.* **21** 4143
Bates D R and McCarroll 1958 *Proc. R. Soc*. A **245** 175
Bugacov A, Maidagan J M, Rivarola R D and Shingal R 1993 *Phys. Rev.* A **47** 1052
Chen Z, Esry B D, Lin C D and Piacentini R D 1994 *J. Phys. B: At. Mol. Opt. Phys.* **27** 2511
Detleffsen D, Anton M, Werner A and Schartner K-H 1994 *J. Phys. B: At. Mol. Opt. Phys.* **27** 4195
Ermolaev A M and McDowell M R C 1987 *J. Phys. B: At. Mol. Phys.* **20** L379

Errea L F, Harel C, Jouin H, Méndez L, Pons B and Riera A 1994b *J. Phys. B: At. Mol. Opt. Phys.* **27** 3603
Errea L F, Méndez L and Riera A 1994a *Phys. Rev.* A **50** 418
Errea L F and Sánchez P 1994 *J. Phys. B: At. Mol. Opt. Phys.* **27** 3677
Fitchard E, Ford A L, and Reading J F 1977 *Phys. Rev.* A **16** 1325
Ford A L, Fitchard E, and Reading J F 1977 *Phys. Rev.* A **16** 133
Ford A L, Reading J F and Becker R L 1982 *J. Phys. B: At. Mol. Phys.* **15** 3257
Ford A L, Reading J F and Hall K A 1993a *J. Phys. B: At. Mol. Opt. Phys.* **26** 4537
—— 1993b *J. Phys. B: At. Mol. Opt. Phys.* **26** 4553
Hall K A, Reading J F and Ford A L 1994 *J. Phys. B: At. Mol. Opt. Phys.* **27** 5257
Henne A, Lüdde H J, Toepfer A, Gluth T and Dreizler R M 1993 *J. Phys. B: At. Mol. Opt. Phys.* **26** 3815
Kuang J, Chen Z and Lin C D 1994 *J. Phys. B: At. Mol. Opt. Phys.* **27** 5731
Kuang Y R 1991a *J. Phys. B: At. Mol. Opt. Phys.* **24** 1645
—— 1991b *J. Phys. B: At. Mol. Opt. Phys.* **24** L103
Lin C D, Soongand S C and Tunnell L N 1978 *Phys. Rev.* A **17** 1646
Martir M H 1981 *Dissertation* Texas A&M University (unpublished)
Phaneuf R A and Janev R K 1993 *Atomic and Plasma-Material Interaction Processes in Controlled Thermonuclear Fusion* ed R K Janev and H W Drawin (Amsterdam: Elsevier) pp371–80
Pechukas P and Light J C 1966 *J. Chem. Phys.* **44** 3897
Rodríguez V D and Miraglia J E 1992 *J. Phys. B: At. Mol. Opt. Phys.* **25** 2037
Shakeshaft R 1978 *Phys. Rev.* A **18** 1930
Slim H A and Ermolaev A M 1994 *J. Phys. B: At. Mol. Opt. Phys.* **27** L203
Wilets L and Gallaher D F 1966 *Phys. Rev* **147** 13
Winter T G 1982 *Phys. Rev.* A **25** 697
—— 1987 *Phys. Rev.* A **35** 3799